nature climate change

LETTERS

PUBLISHED ONLINE: 12 JANUARY 2014 | DOI: 10.1038/NCLIMATE2094

Retreat of Pine Island Glacier controlled by marine ice-sheet instability

L. Favier[1,2], G. Durand[1,2]*, S. L. Cornford[3], G. H. Gudmundsson[4,5], O. Gagliardini[1,2,6], F. Gillet-Chaulet[1,2], T. Zwinger[7], A. J. Payne[3] and A. M. Le Brocq[8]

Over the past 40 years Pine Island Glacier in West Antarctica has thinned at an accelerating rate[1–3], so that at present it is the largest single contributor to sea-level rise in Antarctica[4]. In recent years, the grounding line, which separates the grounded ice sheet from the floating ice shelf, has retreated by tens of kilometres[5]. At present, the grounding line is crossing a retrograde bedrock slope that lies well below sea level, raising the possibility that the glacier is susceptible to the marine ice-sheet instability mechanism[6–8]. Here, using three state-of-the-art ice-flow models[9–11], we show that Pine Island Glacier's grounding line is probably engaged in an unstable 40 km retreat. The associated mass loss increases substantially over the course of our simulations from the average value of 20 Gt yr^{-1} observed for the 1992–2011 period[4], up to and above 100 Gt yr^{-1}, equivalent to 3.5–10 mm eustatic sea-level rise over the following 20 years. Mass loss remains elevated from then on, ranging from 60 to 120 Gt yr^{-1}.

At present Pine Island Glacier (PIG) is responsible for 20% of the total ice discharge from the West Antarctic Ice Sheet[2,3] (WAIS). The accelerated thinning observed since the 1980s has essentially been attributed to enhanced sub-ice-shelf melting[12] induced by the recent alteration of Circumpolar Deep Water circulation[13]. This has reduced the buttressing exerted by the ice shelf, leading to the acceleration of the ice stream and the ongoing retreat of the grounding line along the glacier's trunk observed since 1992[5]. Today the grounding line lies over bedrock that has a steep retrograde slope[14] (Fig. 1c) raising the possibility that PIG may already be engaged in an irrevocable retreat. Assuming that ice flow is dominated by basal sliding and lateral variation can be ignored, grounding lines located on retrograde slopes are always unstable[6,7], but in realistic, three-dimensional geometries lateral drag and buttressing in the ice shelf can act to prevent unstable retreat[11]. Assessing the stability of PIG therefore requires numerical models that accurately represent these additional forces. Models designed to study the evolution of PIG have been reported, though limited to flowline geometries[15] or extreme forcings[8]. Overall, the short-term behaviour of PIG is not well understood and projections vary wildly, ranging from modest retreat to almost full collapse of the main trunk within a century[8,15].

Here, we evaluate the potential instability of PIG and its short-term contribution to sea-level rise (SLR) using state-of-the-art ice-flow models. To decide whether PIG is subject to marine ice-sheet instability (MISI) at present, we must answer two questions: to what extent is the dynamic response of PIG to changes in its ice shelf dictated by the bedrock topography rather than the type and amplitude of the perturbation; and can the grounding line be stabilized on the retrograde slope? Confidence in the answers we propose is of course affected by the accuracy of both the physics implemented in the models that we use and our estimates of poorly constrained parameters. We addressed these questions using three different ice-flow models: the full Stokes model Elmer/Ice[9] and two vertically integrated models: the hybrid (L1L2) model BISICLES[10] and the Shallow Shelf Approximation (SSA) model Úa[11]. All three models participated in the MISMIP3D intercomparison project[16] and showed similar grounding line dynamics, though the SSA solution differed most (Supplementary Section 1.2). Any model of a real glacier suffers from incomplete data sources over and above any shortcomings in model physics: we reflect this inevitable source of error to some extent by getting the three models to make different assumptions about ice viscosity and basal flow conditions (Supplementary Section 3.2).

For all three models, the geometry is relaxed over 15 years to remove unphysical surface undulations induced by remaining uncertainties in the model initial conditions[17]. Surface accumulation is given by the regional atmospheric model RACMO (1980–2004 period[18]) and sub-ice-shelf melting is imposed as a piecewise linear function of water depth with a maximum melting rate of 100 m yr^{-1} below −800 m, linearly decreasing to no melt above −400 m. This melt-rate parameterization, which we will refer to as control, is in reasonable agreement with the amplitude and the enhanced melting close to the grounding line that are inferred from observations[19], but is clearly less sophisticated than coupling with an ocean circulation model, as for example in ref. 20. The resulting initialization procedure leads to good agreement with observations for the three models, with a contribution to SLR comparable to the average estimate of about 20 Gt yr^{-1} over the past 20 years[4]. Afterwards, the contribution remains similar during the 50 years of the control run (Fig. 2). The initial state of each model is described in more detail in the Supplementary Section 4.2.

The recent retreat of PIG is now firmly attributed to acceleration of the glacier in response to sub-ice-shelf melting. To evaluate the consequences of melting on PIG dynamics, four different melt-rate perturbations are tested. These are described in detail in the Supplementary Section 3.3, but in brief, m1 doubles the peak melt rate of control, m2 extends the region of melting to a larger portion of the ice shelf, m3 does both and m4 is initially the same as m2 but is limited to the region of the present-day ice shelf even

[1]CNRS, LGGE, Grenoble F-38041, France, [2]Univ. Grenoble Alpes, LGGE, Grenoble F-38041, France, [3]School of Geographical Sciences, University of Bristol, BS8 1SS, UK, [4]British Antarctic Survey, Natural Environment Research Council, Madingley Road, Cambridge CB3 0ET, UK, [5]CAREERI, Chinese Academy of Sciences, Lanzhou 730000, China, [6]Institut Universitaire de France, 103 bd St Michel, 75005 Paris, France, [7]CSC-IT Center for Science Ltd, PO Box 405, FIN-02101 Espoo, Finland, [8]Geography, College of Life and Environmental Sciences, University of Exeter, Rennes Drive, Exeter EX4 4RJ, UK.
*e-mail: durand@lgge.obs.ujf-grenoble.fr

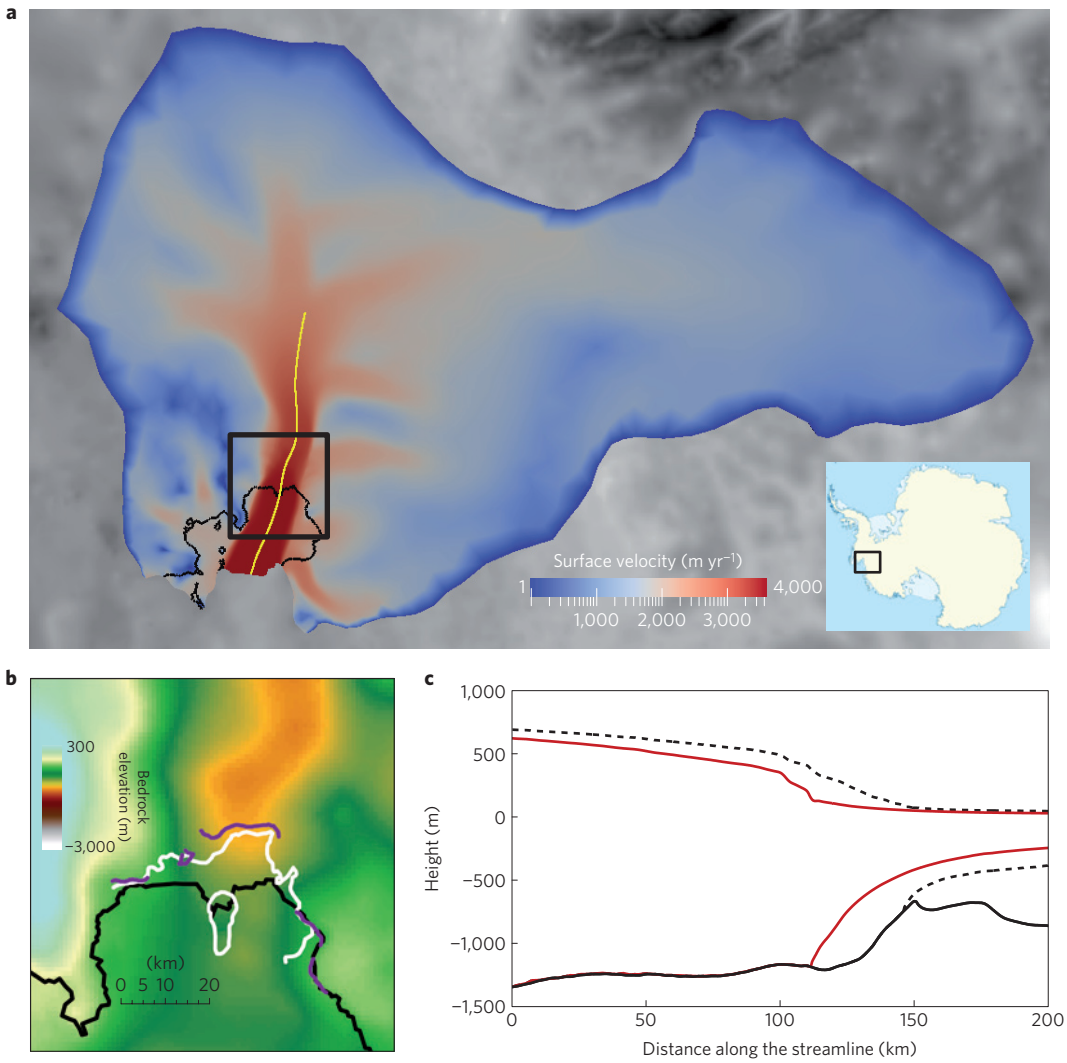

Figure 1 | PIG location and geometry. a, Relaxed surface velocities plotted on the Elmer/Ice computational domain, the solid black line represents the relaxed grounding line. **b**, Domain zoom-in with the bedrock elevation (in m). The 2011 grounding line from ref. 5 is shown in purple, the 2009 grounding line from ref. 8 is in white. **c**, Geometry of PIG produced by Elmer/Ice along the yellow flowline shown in **a** at time (t) = 0 (dotted line) and after 50 years under melting scenario m2 (red line).

if the grounding line retreats. The amplitudes of these melt-rate perturbations are plausible when compared with observational and modelling results[19,21]; Supplementary Section 2.2). For Elmer/Ice, the m1 melt-rate distribution does not alter the grounding line position but the remainder leads to significant retreat. BISICLES exhibits retreat in all four cases, but the response to m1 is delayed by 20 years. Once Elmer/Ice and BISICLES have started to retreat, they behave similarly. The grounding line retreats by 40 km over the retrograde slope within a few years and the rate of contribution to SLR reaches a peak of almost 130 Gt yr^{-1} (Fig. 2), after which the rate of retreat diminishes. The associated rate of contribution to SLR also reduces after the rapid retreat but mass imbalance remains elevated, at between 60 and 120 Gt yr^{-1}, that is, 3–6 times higher than before the perturbation was imposed. Imbalance estimations made by BISICLES are generally higher than those made by Elmer/Ice: the grounding line of the former model being more prone to continued retreating over gentle slopes. BISICLES is indeed known to react slightly faster than Elmer/Ice[16]; alternatively the spatial resolution of Elmer/Ice may be insufficient to properly model a moderate retreat rate (details in the Supplementary Section 4.1). We see similar patterns of retreat when we consider different perturbations, such as calving events (Supplementary Section 4.1), or alternative melt-rate parameterizations (Supplementary Section 5.2). The response to the melt-rate perturbations is different for Úa as m1 and m3 lead to substantial retreat, whereas m2 leads to less of a response. Once retreat starts, though, the Úa's grounding line steadily retreats and the contribution to SLR continuously increases up to 250 Gt yr^{-1}, leading to a rapid collapse of the main trunk. The faster retreat computed by Úa might be explained by the SSA model itself[16], but also might be related to the model's parameters. For example, Úa computes the fluidity, A, and hence the effective viscosity, in a different way (Supplementary Section 3.2). Viscous stresses play a vital role in the dynamics close to the grounding line but are much less important far from it[6], so that models with quite different viscosity can reproduce the observed velocity equally well, but diverge from one another as the grounding line retreats.

We explore the degree of irreversibility further by carrying out experiments where the melt rate is reduced as soon as the PIG grounding line starts retreating. In each experiment, the most moderate perturbation that leads to retreat (m2 for Elmer/Ice and BISICLES and m1 for Úa) is applied until the acceleration of the

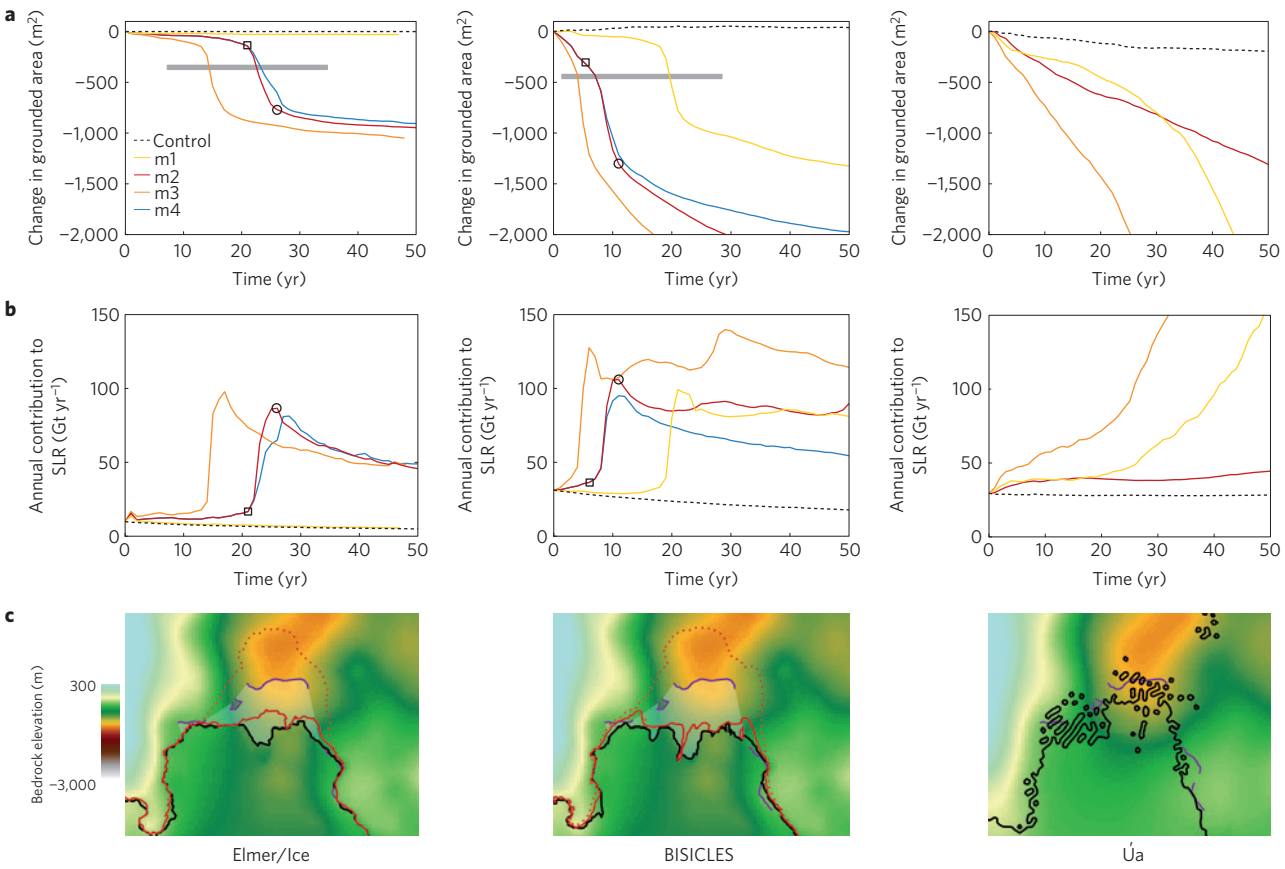

Figure 2 | Melting experiments. a–c, Results of the melting experiments for Elmer/Ice (left), BISICLES (middle) and Úa (right, for which m4 is similar to m2 and not therefore visible) for: change in grounded areas (**a**) and annual contribution to SLR (**b**). Elmer/Ice and BISICLES respond to enhanced melting with a rapid retreat across the steep reverse slope followed by slower retreat thereafter, whereas Úa increases its rate of retreat throughout the simulations. The bedrock altitude (m) and the initial grounding lines for each model (solid black line), as well as the grounding lines, computed during the m2 experiment, at the beginning (solid red lines) and at the end (dashed red line) of the rapid retreat for Elmer/Ice and BISICLES (Úa is not shown here because of the difficulty of identifying these two times) are shown in **c**. Corresponding times are indicated by a square and a circle respectively in **a**,**b**. **c** also shows the areas (shaded) separating the grounding line as observed in 2011 (purple line[5]) from the relaxed model grounding lines, which cover $364 \pm 50\,km^2$, $426 \pm 50\,km^2$ for Elmer/Ice and BISICLES, respectively (not shown for Úa because of the non-continuous profile of the grounding line). The thick grey lines in **a** indicate the same area.

dynamic contribution to SLR reaches a maximum, at which point the melt rate reverts to control. For Elmer/Ice and BISICLES, this slightly impacts ice dynamics: the grounding line keeps retreating and the imbalance is not significantly affected when crossing the bedrock steep retrograde slope area. However, it does limit both further retreat and the imbalance that persists once the bottom of the trench is reached (Fig. 3). Úa behaves quite differently, with the grounding line returning to its original location after an initial retreat across the retrograde slope. We examine further the conditions under which a complete reversal could occur by conducting similar experiments where the melt rate is reduced to 75, 50, 25, 10 or 5% of control. The glacier recovers its initial state in all of the Úa simulations, but only when the melt rate is reduced to 10% of control or less for Elmer/Ice and 25% or less for BISICLES. Most notably, none of the models produces a steady grounding line on the reverse slope. Further experiments along these lines are described in the Supplementary Section 5.2.

We find that readvance takes place because a large reduction of melt rates lowers the bottom surface, which then regains contact with elevated points on the bedrock. Grounded pinning points increase the buttressing force exerted by the ice shelf, reduce imbalance and may slow down the grounding line retreat and possibly induce a readvance of the grounding line. Note that the presence of pinning points is not a sufficient condition for stabilizing the ice sheet; the MISI may still occur if only weak grounded pinning points have been formed (Fig. 3). As the initial position of the grounding line before perturbation can be regained only if the melt rate is reduced substantially and to far less than the value observed at present, reversibility of the present retreat of PIG looks unlikely.

Here we show that for the next decade the PIG grounding line is probably engaged in an irreversible retreat over tens of kilometres and that the dynamic contribution to SLR will remain at a significantly higher level compared with preretreat conditions. All three models, despite their differing physics, numerics and parameters, support the notion of MISI in PIG, and two out of three cast doubt on any possible recovery. Starting from the first years of significant imbalance increase, the variation of the mass loss between experiments after 20 years is relatively narrow with a cumulative contribution to SLR of 3.5–10 mm over this period (Fig. 4). Afterwards, estimates diverge dependent on further retreat of the grounding line across a region of gentler slopes and stronger basal traction behind the instability zone. Once the grounding line has crossed the steep retrograde slope, imbalance decreases but remains between three and six times higher than the mean estimates obtained for the past 20 years ($20\,Gt\,yr^{-1}$; ref. 4).

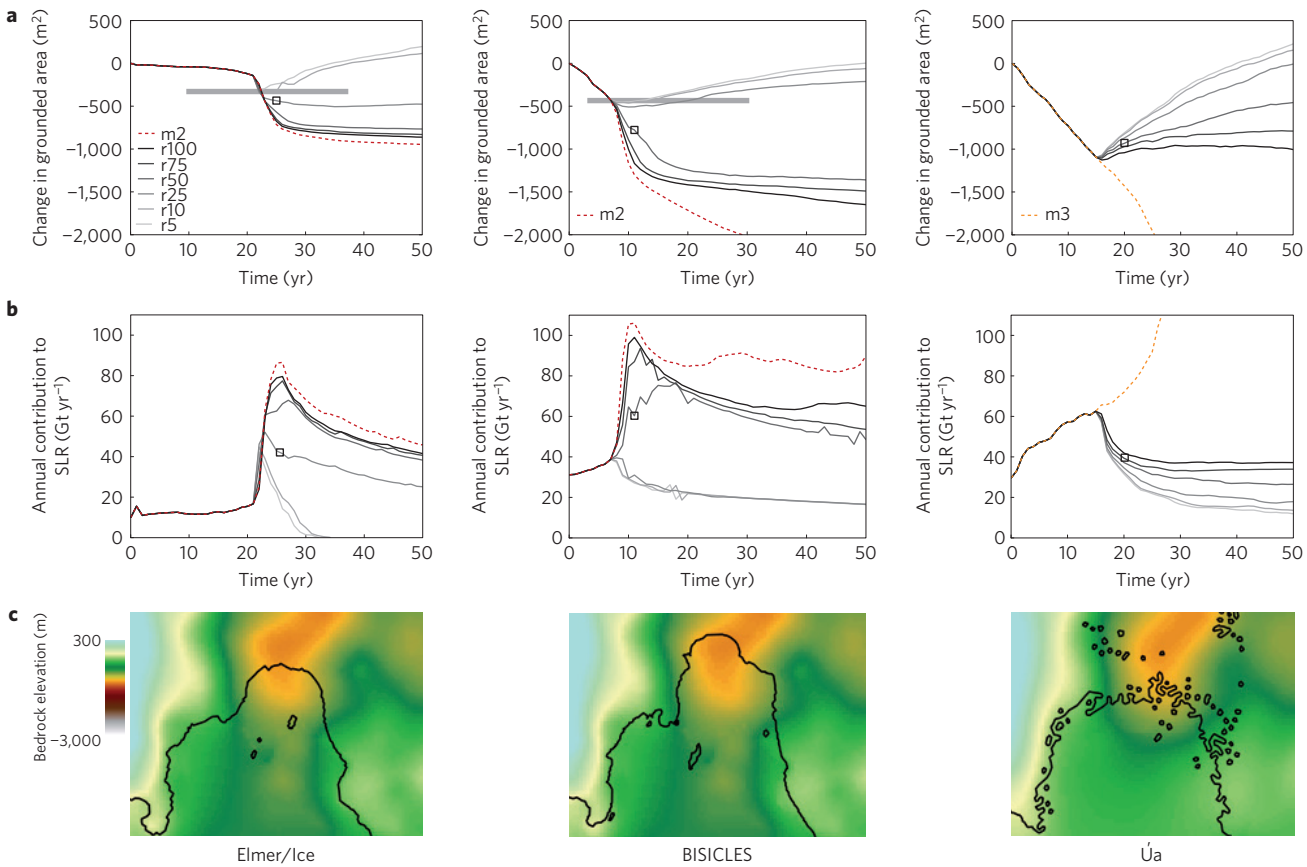

Figure 3 | Reverse experiments. a–c, Retreat reversibility experiments starting from the m2 experiment for Elmer/Ice (left) and BISICLES (middle) and from the m3 experiment for Úa (right), in terms of change in grounded areas (**a**) and annual contribution to SLR (**b**). The legend for the reverse experiments applies to all panels in **a** and **b**; r100, r75, r50, r25, r10 and r5 indicate a reduced rate to a percentage of the control run, respectively. **c** shows the bedrock (in m) with grounding lines taken at times symbolized by a square in the upper rows. The thick horizontal grey line in **a** is reproduced from Fig. 2 and represents the 2011 grounding line observed by ref. 5. The Elmer/Ice r25 simulation does eventually retreat across the MISI zone (as shown in the Supplementary Fig. 14).

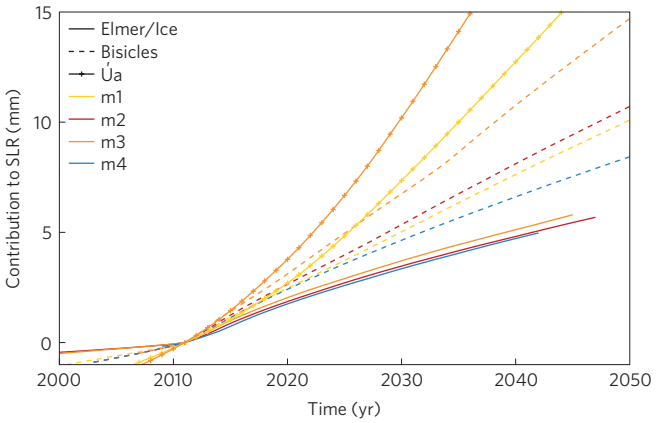

Figure 4 | Integrated contribution to SLR for melting experiments that produces a grounding line retreat. The results have been shifted to equal a null contribution for 2011, which is also the year of the last measured grounding line[5]. The corresponding offsets were estimated from the intersection between thick grey lines and changes in grounded areas from Fig. 2a.

Methods

Models and numerics. Simulations were carried out with three ice-flow models. Elmer/Ice[9] solves the full Stokes set of equations in three-dimensional, BISICLES (ref. 10) and Úa (ref. 11) are based on L1L2 (ref. 22) and SSA (ref. 23) models, respectively, and solve simplified vertically integrated equation sets that retain all but vertical shear stress terms, which are ignored in the SSA model and parameterized in the L1L2 model. Elmer/Ice applies a finite element method on a fixed and horizontally unstructured locally refined grid, BISICLES a finite volume method on a block-structured adaptive mesh and Úa a finite element method on a refined grid.

Inputs. Elmer/Ice and BISICLES interpolate topographic data from a 1 km mesh grid version of the ALBMAP data set, computed using similar methods described in ref. 24. Temperatures were computed on a 5 km grid in ref. 25 and do not evolve with time. Surface velocities were acquired during the last International Polar Year[26] and accumulation rates are given by regional atmospheric modelling[18]. In Úa the topography is constrained using bedrock[27] and surface altitude data sets and ice-shelf thickness[28] data sets, surface velocities are given by ref. 29 and surface accumulation by ref. 30.

Received 24 May 2013; accepted 4 December 2013; published online 12 January 2014

References

1. Bindschadler, R. History of lower Pine Island Glacier, West Antarctica, from Landsat imagery. *J. Glaciol.* **48,** 536–544 (2002).
2. Rignot, E. *et al.* Recent antarctic ice mass loss from radar interferometry and regional climate modelling. *Nature Geosci.* **1,** 106–110 (2008).
3. Wingham, D., Wallis, D. & Shepherd, A. Spatial and temporal evolution of Pine Island Glacier thinning, 1995–2006. *Geophys. Res. Lett.* **36,** L17501 (2009).
4. Shepherd, A. *et al.* A reconciled estimate of ice-sheet mass balance. *Science* **338,** 1183–1189 (2012).
5. Park, J., Gourmelen, N., Shepherd, A., Kim, S., Vaughan, D. & Wingham, D. Sustained retreat of Pine Island Glacier. *Geophys. Res. Lett.* **40,** 2137–2142 (2013).
6. Schoof, C. Ice sheet grounding line dynamics: Steady states, stability, and hysteresis. *J. Geophys. Res.* **112,** F03S28 (2007).

7. Durand, G., Gagliardini, O., de Fleurian, B., Zwinger, T. & Le Meur, E. Marine ice sheet dynamics: Hysteresis and neutral equilibrium. *J. Geophys. Res.* **114,** F03009 (2009).
8. Joughin, I., Smith, B. E. & Holland, D. M. Sensitivity of 21st century sea level to ocean-induced thinning of Pine Island Glacier, Antarctica. *Geophys. Res. Lett.* **37,** L20502 (2010).
9. Favier, L., Gagliardini, O., Durand, G. & Zwinger, T. A three-dimensional full stokes model of the grounding line dynamics: Effect of a pinning point beneath the ice shelf. *Cryosphere* **6,** 101–112 (2012).
10. Cornford, S. *et al.* Adaptive mesh, finite volume modeling of marine ice sheets. *J. Comput. Phys.* **232,** 529–549 (2013).
11. Gudmundsson, G., Krug, J., Durand, G., Favier, L. & Gagliardini, O. The stability of grounding lines on retrograde slopes. *The Cryosphere* **6,** 1497–1505 (2012).
12. Pritchard, H. *et al.* Antarctic ice-sheet loss driven by basal melting of ice shelves. *Nature* **484,** 502–505 (2012).
13. Jacobs, S., Jenkins, A., Giulivi, C. & Dutrieux, P. Stronger ocean circulation and increased melting under Pine Island Glacier ice shelf. *Nature Geosci.* **4,** 519–523 (2011).
14. Vaughan, D. *et al.* New boundary conditions for the West Antarctic ice sheet: Subglacial topography beneath Pine Island Glacier. *Geophys. Res. Lett.* **33,** L09501 (2006).
15. Gladstone, R. M. *et al.* Calibrated prediction of Pine Island Glacier retreat during the 21st and 22nd centuries with a coupled flowline model. *Earth Planet. Sci. Lett.* **333,** 191–199 (2012).
16. Pattyn, F. *et al.* Grounding-line migration in plan-view ice-sheets models: Results of the ice2sea mismip3d intercomparison. *J. Glaciol.* **59** (215), 410–422 (2013).
17. Gillet-Chaulet, F. *et al.* Greenland ice sheet contribution to sea-level rise from a new-generation ice-sheet model. *Cryosphere* **6,** 1561–1576 (2012).
18. Van de Berg, W., van den Broeke, M., Reijmer, C. & van Meijgaard, E. Reassessment of the antarctic surface mass balance using calibrated output of a regional atmospheric climate model. *J. Geophys. Res.* **111,** D11104 (2006).
19. Dutrieux, P. *et al.* Pine Island Glacier ice shelf melt distributed at kilometre scales. *The Cryosphere* **7,** 1543–1555 (2013).
20. Goldberg, D. *et al.* Investigation of land ice–ocean interaction with a fully coupled ice-ocean model: 1. Model description and behaviour. *J. Geophys. Res.* **117,** F02037 (2012).
21. Payne, A. J. *et al.* Numerical modeling of ocean–ice interactions under Pine Island Bay's ice shelf. *J. Geophys. Res.* **112,** C10019 (2007).
22. Schoof, C. & Hindmarsh, R. Thin-film flows with wall slip: An asymptotic analysis of higher order glacier flow models. *Q. J. Mech. Appl. Math.* **63,** 73–114 (2010).
23. MacAyeal, D. Large-scale ice flow over a viscous basal sediment-theory and application to ice stream B, Antarctica. *J. Geophys. Res.* **94,** 4071–4087 (1989).
24. Le Brocq, A., Payne, A. & Vieli, A. An improved Antarctic dataset for high resolution numerical ice sheet models (ALBMAP v1). *Earth Syst. Sci. Data* **2,** 247–260 (2010).
25. Pattyn, F. Antarctic subglacial conditions inferred from a hybrid ice sheet/ice stream model. *Earth Planet. Sci. Lett.* **295,** 451–461 (2010).
26. Rignot, E., Mouginot, J. & Scheuchl, B. Ice flow of the Antarctic ice sheet. *Science* **333,** 1427–1430 (2011).
27. Timmermann, R. *et al.* A consistent data set of Antarctic ice sheet topography, cavity geometry, and global bathymetry. *Earth Syst. Sci. Data* **2,** 261–273 (2010).
28. Ligtenberg, S., Helsen, M. & van den Broeke, M. An improved semi-empirical model for the densification of Antarctic firn. *The Cryosphere* **5,** 809–819 (2011).
29. Joughin, I. *et al.* Basal conditions for Pine Island and Thwaites Glaciers, West Antarctica, determined using satellite and airborne data. *J. Glaciol.* **55,** 245–257 (2009).
30. Lenaerts, J., van den Broeke, M., van de Berg, W. J., van Meijgaard, E. & Kuipers Munneke, P. A new, high-resolution surface mass balance map of Antarctica (1979–2010) based on regional atmospheric climate modeling. *Geophys. Res. Lett.* **39,** L04501 (2012).

Acknowledgements

We are grateful to T. Flament for observations of surface elevation change, A. Shepherd and N. Gourmelen for recent location of the grounding line and P. Dutrieux for discussions on sub-ice-shelf melting. Elmer/Ice computations were carried out using HPC resources from GENCI-CINES (grant/2012016066/) and from the Service Commun de Calcul Intensif de l'Observatoire de Grenoble (SCCI). BISICLES calculations were carried out on the University of Bristol's Blue Crystal Phase 2 supercomputer and the code is jointly developed with D. F. Martin at Lawrence Berkeley National Laboratory, California, USA, with financial support provided by the US Department of Energy and the UK Natural Environment Research Council. This work was supported by financial support from the ice2sea program from the European Union 7th Framework Programme, grant number 226375, ice2sea contribution number 157 and by NERC grant number NE/H02333X/1.

Author contributions

L.F. and G.D. designed the experiments. L.F. did the numerical modelling with Elmer/Ice, S.L.C. with BISICLES and G.H.G. with Úa. O.G., F.G-C. and T.Z. contributed to the set-up of Elmer/Ice, A.J.P. contributed to BISICLES. A.M.L.B. provided the high-resolution topographic input data set that has been used by Elmer/Ice and BISICLES. L.F., G.D. and S.L.C. led the writing of the manuscript, which has been improved by all authors.

Additional information

Supplementary information is available in the online version of the paper. Reprints and permissions information is available online at www.nature.com/reprints. Correspondence and requests for materials should be addressed to G.D.

Competing financial interests

The authors declare no competing financial interests.